Colloids and Surfaces A: Physicochemical and Engineering Aspects 686 (2024) 133375

Contents lists available at ScienceDirect

Colloids and Surfaces A: Physicochemical and Engineering Aspects

journal homepage: www.elsevier.com/locate/colsurfa

Sodium lauryl ether sulfates, pivotal surfactants for formulations: Rationalization of their assembly properties

Rosaceleste Zumpano [a], Alessandra Del Giudice [b], Stefano Resta [c], Andrea D'Annibale [b], Fabio Sciubba [d,e], Francesco Mura [f], Giacomo Parisi [f], Maria Chiara di Gregorio [b,*], Luciano Galantini [b,*]

[a] Department of Chemistry and Drug Technologies, Sapienza University of Rome, P.le Aldo Moro 5, 00185 Rome, Italy
[b] Department of Chemistry, Sapienza University of Rome, P.le A. Moro 5, 00185 Rome, Italy
[c] Fater SpA, Via Mare Adriatico 122, 65010 Spoltore, Pescara, Italy
[d] Department of Environmental Biology, Sapienza University of Rome, P.le A. Moro 5, 00185 Rome, Italy
[e] NMR-Based Metabolomics Laboratory (NMLab), Sapienza University of Rome, P.le A. Moro 5, 00185 Rome, Italy
[f] Department of Basic and Applied Sciences for Engineering (SBAI), Sapienza University of Rome, Via Antonio Scarpa, 14, 00161 Rome, Italy

GRAPHICAL ABSTRACT

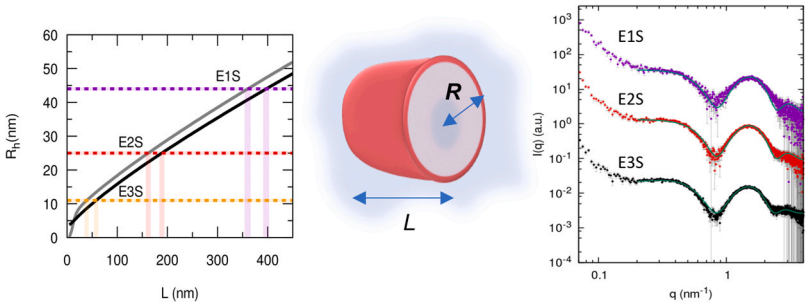

ARTICLE INFO

Keywords:
SLES
Surfactants
SAXS
Dynamic light scattering
Self-assembly

ABSTRACT

Hypothesis: Sodium lauryl ether sulfates (SLES) are a class of surfactants, among the most used in the formulations of healthcare products. Although largely used in industry, literature studies are hereto completely missing of the characterization of some species, as sodium lauryl triether sulfates (**E3S**), and of the effect of several assembly parameters, as temperature. Moreover, drastic disparity of assembly performance subsists among laboratory synthesized and industrial raw SLES, generating problems in the real-world applications of formulations design.

Experiments: We report on the self-assembly analysis of industrial grade sodium lauryl monoether sulfate (**E1S**), sodium lauryl diether sulfate (**E2S**) and laboratory synthesized **E3S**. The surfactants were studied in a large range of NaCl concentrations (0.1–1 M NaCl) and as function of the temperature by crossing Surface Tension, Small-Angle X-ray Scattering and Dynamic Light Scattering measurements.

Findings: Such analysis enabled to establish systematic relationship between the molecular structure and assembly properties of the surfactants and to define size and morphologies variations of the aggregates. We

* Corresponding authors.
E-mail addresses: mariachiara.digregorio@uniroma1.it (M.C. di Gregorio), luciano.galantini@uniroma1.it (L. Galantini).

https://doi.org/10.1016/j.colsurfa.2024.133375
Received 26 July 2023; Received in revised form 10 January 2024; Accepted 31 January 2024
Available online 3 February 2024

observed that i) core-shell spherical aggregates evolve towards elongated core-shell structures upon addition of NaCl, ii) the elongation is higher the lower the number of the ether groups iii) **E3S** is greatly stable in the analyzed temperature range (20 °C - 60 °C), iv) the industrial grade **SLES** exhibit a minimum of the surface tension and an anticipated self-assembly as a function of concentration, probably due to the presence of hydrophobic impurities. Impurities are also detected by DLS in unfiltered samples of the industrial grade **SLES** as large particles.
Moreover, a case of industrial interest was investigated: the instability of formulations comprising of **E3S** and 3,4,5-trimethoxybenzoic acid.
Such information enriches the quite small literature on pure SLES self-assembly, rationalizing new and literature data within a unified framework.

1. Introduction

Rationalization of surfactant assembly is crucial for the efficacy of many commercial products and industrial processes, since surfactants are involved in different aspects of the market [1–3], from detergents [4,5], nanomaterials [6–9] and drug [10–12] production to petroleum industry [13,14]. To optimize their activity as soaps, emulsifying and solubilizing agents, it is equally important to understand how the molecular structure design and the co-work with other formulation molecules affect the assembly properties.

Sodium lauryl ether sulfates, commonly known by the acronym of SLES, have been of great importance in the economical, chemical and industrial scenario of the last sixty years [15]. They show numerous properties as highly foaming capacity, stability in hard water and excellent emulsifying and solubilizing activity towards organic molecules [16]. For these reasons, after 1950, SLES has been replacing soaps of natural origin, becoming among the most used synthetic surfactants in the formulations of detergents, cosmetics and healthcare products. Their molecular structure is formed by a chain of twelve carbon atoms and a hydrophilic area comprising of a charged sulphate head connected to one or more ethoxyl groups (in the following text the abbreviation **EnS** will be used to indicate SLES with a n number of ether groups). Industrial SLES synthesis is cheap and performed on a large scale by ethoxylation of the dodecanol and subsequent conversion of the ethoxylate form into sulfate ester. This process leads to a final product that is a distribution of SLES with different degrees of ethoxylation. Generally, they are commercially labelled referring to the average number of the ether groups in the SLES distribution [17].

In the formulation of personal care products SLES coexist with other molecular classes that are used complementary as stabilizers, dyes, perfuming agents, modulators of rheological and foam properties etc [18–20]. The need to optimize more and more such formulations has promoted the physical-chemical investigations of composite systems where SLES assembly is studied in the presence of additives. To mention some examples, synergistic effects were studied in multi-component SLES systems comprising of fatty alcohols [21,22], fatty acids [23,24], biosurfactants [25], polyelectrolytes [26], and foam boosters [27,28]. However, systematic studies of single component SLES systems are less common [19]. Zoeller and Blankschtein studied laboratory synthesized SLES with numbers of oxyethylene units of 1,2,4,5 and 6. The surfactant concentration was set at 0.05 M and addition of NaCl were performed in a 0.1 M-0.6 M range [29]. Diffusion, viscosity, and density measurements have been performed by Tokiwa and Ohki on a series of SLES with oxyethylene units from 1 to 10 with an added concentration of 0.10 M NaCl [30]. Parker and Fieber analyzed the viscoelastic properties of **E2S** in NaCl solutions [31].

In this work, we contribute to enlarge the understanding of single component SLES systems, investigating the assembly properties of industrial grade **E1S**, **E2S, E3S** in NaCl solutions. In addition, pure (laboratory synthesized) E3S was also characterized. Unlike the reported literature, the compounds were studied by dynamic light scattering (DLS) and small angle X-ray scattering (SAXS) by analyzing: i) lower surfactant concentration (0.03 M), ii) a larger range of NaCl concentration (0.1–1 M), iii) temperature effect. Moreover, mixtures of **E3S** and increasing concentration of 3,4,5-trimethoxybenzoic acid (**TMBA**) were investigated. **TMBA** is a hydrotropic molecule usually added in commercial cleaners as stabilizer [32,33]. Hydrotropes are a class of amphiphilic molecules capable to solubilize hydrophobic molecules in water by a different mechanism than micellar solubilization [34,35]. Unlike micelle assembling surfactants, hydrotropes do not have a critical micellar concentration due to not extended hydrophobic area which hinders the spontaneous self-aggregation. However, they assemble when a hydrophobic solute is present and they can drastically change the aggregation properties of conventional surfactants even at low concentration. This specific study is motivated by a general issue in the industrial production of detergents, as it has been observed that detergents comprising **E3S** and **TMBA** go often through a time dependent phase separation process.

2. Materials and methods

2.1. Materials

NaCl was purchased by Carlo Erba and used without further purification. Industrial grade **E1S** and **E2S** were provided by Fater S.p.A. as a water solution (95 wt% and 27 wt% for **E1S** and **E2S**, respectively). Two different products of **E3S** were used in the analysis. Industrial grade **E3S** was provided by Fater SpA as a water solution (28 wt%). Such material is a mixture of SLES with different degrees of ethoxylation. The composition is reported in (Table 1).

Industrial grade **E3S** samples were used for DLS analyses and for the SAXS investigation. Pure **E3S** was synthesized according to the procedure reported in the next paragraph. This material was used for the samples in NaCl 6% solution and in combination with TMBA that were analyzed by NMR and SAXS. Additional SAXS measurements and surface tension measurements were performed on highly pure **E2S** (purity 95%)

Table 1
Composition of the industrial grade E3S.

EnS, n = number of ether groups	mol%
E0S	16.74
E1S	10.90
E2S	12.62
E3S	12.44
E4S	10.74
E5S	8.83
E6S	6.96
E7S	5.61
E8S	4.40
E9S	3.34
E10S	2.49
E11S	1.74
E12S	1.2
E13S	0.79
E14S	0.51
E15S	0.31
E16S	0.18
E17S	0.1
E18S	0.05
E19S	0.03

and **E3S** (purity 95%) acquired from Merck and Angene Chemical, respectively.

2.2. E3S synthesis

For the synthesis of **E3S**, 1- bromododecane (97%), trietilenglicole (99%), sodium hydride (60% dispersion in mineral oil) and chlorosulfonic acid (99%) were purchased by Sigma Aldrich and used without further purification.

The synthetic procedure comprises of two steps as reported in Scheme 1:

Synthesis of [2-[2-(2-dodecyloxy)- ethoxy]ethanol] (2): Trietilenglicole (16.67 g) and sodium hydride (0.50 g) were reacted in a three-neck round-bottom flask (capacity 50 ml) in inert atmosphere for 1 h, at room temperature, under stirring. Subsequently, 1-bromododecane (4.152 g) was added. The mixture was heated up to 60 °C and was kept in inert atmosphere for 24 h under stirring. The reaction was monitored by thin layer chromatography (eluent DCM / ether = 8: 2). Then the reaction was stopped after 24 h by adding 20 ml of distillated water and stirring for 5 min. The obtained solution was transferred in a separation funnel. Extraction was performed with ethyl ether (50 ml x 3). The organic phase was collected and dried over anhydrous sodium sulphate. Subsequently, the solvent was removed under reduced pressure to obtain a yellowish oil (4.73 g). The so obtained product was purified by silica gel column chromatography (elution solvents: gradient from pure DCM up to solvent mixture of DCM/ether=8:2). The eluate was evaporated to obtain [2-[2-(2-dodecyloxy)- ethoxy]ethanol] (transparent oil, 3.5 g, yield 66%). Characterizing spectra of the compound are reported in Fig. S1.

*Synthesis of **E3S***: [2-[2-(2-dodecyloxy)- ethoxy]ethanol] (0.2 g) was dissolved in DCM (3 ml). Chlorosulfonic acid (0.24 g) was added to DCM (3 ml). The chlorosulfonic acid solution was dropped in the DCM solution of [2-[2-(2-dodecilossi)- etossi]etanolo] and kept under stirring for about 30 min. The reaction is monitored by thin layer chromatography. Subsequently, NaOH 0.1 M was added and the obtained solution was evaporated under reduced pressure to attain the final product (white solid, 0.18 g, yield 72%) MW= 420 g/mol, critical micellar concentration = 2.8 mM at 25 °C, Kraft point lower than 0 °C. Characterizing spectra of E3S are reported in Fig. S2.

2.3. Sample preparation

Stock solutions of SLES were prepared at a concentration of 2 wt% by dilution of the samples furnished by the company or by solubilization of the synthesized **E3S** in bidistilled water. Stock solution of NaCl in water was prepared at a concentration of 12 wt% by dissolving NaCl powder in bidistilled water. The samples for the analysis were prepared by mixing the SLES and NaCl stock solutions in the right proportions. Further dilution by water was performed up to reach the desired volume and concentration when needed. For DLS and SAXS analysis, the samples were filtered 3 times by a hydrophilic filter (Syringe Filters – Cellulose Acetate, Millipore Durapore 0.1 μm).

Table 2 provides the concentrations of SLES and NaCl with the related significant figures that are used for the samples'preparation. The standard deviations for each concentration are within 0.5%.

Table 2
Concentration of SLES and NaCl used in the samples' preparation.

COMPOUND	wt%
E2S (mother solution)	28.0
E3S (mother solution)	28.0
E2S	1.00
E3S	1.00
NaCl	0.500
	2.50
	6.00

2.4. Dynamic light scattering (DLS)

DLS measurements were carried out by a Brookhaven Instruments and a Malvern Nano-Zeta Sizer (for the temperature trends).

The Brookhaven instrument enables to collect the light scattered by a sample at variable angles. It is equipped with a BI2030AT digital correlator with 136 channels, a BI200SM goniometer and a laser operating at 532 nm. The reported measurements were collected at 90°. The samples were thermostated at 25 ± 0.5 °C by a circulating water bath. The Malvern Nano-ZetaSizer is equipped with a 5 mW HeNe laser (λ = 632.8 nm) and a digital logarithmic correlator. The normalized intensity autocorrelation functions are measured at a fixed angle of 173°. The autocorrelation functions were analyzed by using the cumulant fit method. The apparent diffusion coefficients of the particles were achieved from the first cumulant and converted into apparent hydrodynamic diameter (DH) using the Stokes–Einstein equation.

2.5. Small angle X-ray scattering (SAXS)

Small angle X-ray scattering (SAXS) measurements were performed at MAX II SAXS beamline I911–4 at the MAXIV Laboratory in Lund, Sweden [36]. The X-ray scattering intensity was recorded at a wavelength = 0.091 nm on a 165-mm-diameter MarCCD detector, which was placed at a sample-to-detector distance of 2.311 m. The corresponding range of scattering vector $q = 4\pi\sin\theta/\lambda$ (with 2θ the scattering angle and λ the photon wavelength), was 0.057 – 4 nm^{-1} and was calibrated using silver behenate as a standard. The samples were loaded into sealed quartz capillary cells. The two-dimensional SAXS patterns were processed using Fit2D software [37]. The temperature was kept at 25 ± 0.5 °C using a capillary holder connected with an external heating bath.

Additional measurements were performed at SAXSLab Sapienza with a Xenocs Xeuss 2.0-QXoom, with a X-ray source wavelength = 0.1542 nm, a collimated beam of 0.5 mm × 0.5 mm and a Pilatus3 R300K detector, placed at a sample-to-detector distance of 0.55 m. The corresponding range of q was 0.13 – 6 nm^{-1}. The samples were loaded into disposable glass capillaries with internal diameter 1.5 ± 0.2 mm whose thickness was estimated in the alignment scans and measured at room temperature (25–26 °C). The two-dimensional scattering patterns collected with a total acquisition time of 3 h were subtracted for the "dark" counts, and then masked, azimuthally averaged, and normalized for transmitted beam intensity, exposure time and subtended solid angle per pixel, using the FOXTROT software developed at SOLEIL.

The azimuthally integrated scattering profiles of the samples were

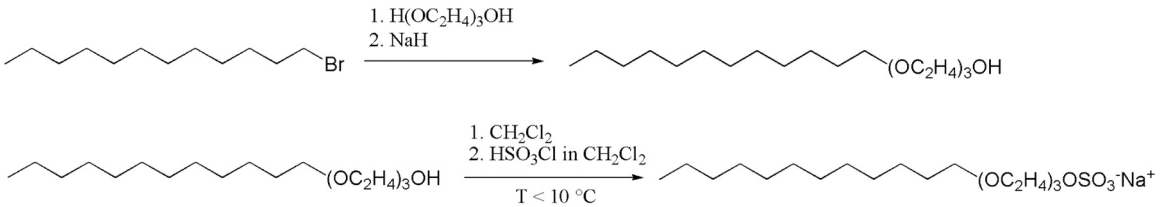

Scheme 1. Synthetic steps for the preparation of E3S.

corrected for scattering contributions of the capillary and the solvent (NaCl water solutions) and thereafter put on an absolute scale using pure water as a calibration standard [38]. The indirect Fourier transform to obtain the pair distance distribution functions in the real space by fitting the experimental SAXS profiles was performed with BayesApp [39]. Analytical models were calculated with SasView 5.0.5 [40] and SASfit 0.94.12 [41].

2.6. Nuclear magnetic resonance (NMR) spectroscopy

NMR spectra were carried out on a Bruker Avance III 400 spectrometer operating at a frequency.

of 400.13 MHz for the proton. **E3S** and **TMBA** were solubilized in 0.5 ml of deuterium oxide. Monodimensional ^{1}H experiments were acquired employing the *presat* pulse sequence with 64 K data points, 16 scans, a spectral width of 15 ppm, a recycle delay of 5 s and a solvent presaturation time of 2 s. Pseudo bidimensional DOSY experiments were acquired employing the *ledbpgp2s* pulse sequence with 64 K data points, 32 scans, a spectral width of 15 ppm, 32 gradient increments, a diffusion time of 150 ms, a gradient length of 1500 μs and a recycle delay of 2 s

2.7. Surface tension measurements

The surface tension γ as a function of concentration was measured by the ring detachment method on water solutions of **E2S** and **E3S** and the results for pure commercial products and the industrial grade mixtures were compared. Measurements were performed with a computerized Lauda instrument maintaining the temperature at 25.0 ± 0.1 °C by a thermostatic apparatus. The cac values were inferred from the breakpoints in the γ vs logarithm(surfactant concentration) curves.

2.8. Transmission electron microscopy (TEM)

TEM images were collected on **E3S** 1 wt% in water and in NaCl 6 wt %.

The TEM grids required two different preparations. 10 μl of **E3S** 1 wt % in NaCl 6 wt% was drop-casted on the TEM grid (carbon film coated Cu grid, 300 mesh) and the excess drop was blotted after 10 s. This rapid procedure reduces the possibility of local concentration increase, structure aggregation or NaCl crystal formation due to the drop evaporation.

The same grid preparation was tried also for **E3S** 1 wt% in water but none structures could be imaged because probably the structures are less stable in absence of ionic strength.

Therefore, 5 μl of **E3S** 1 wt% in water was drop-casted on the TEM grid and the drop was left to air-dry without blotting. This procedure probably allowed for a steadier adhesion on the grid of the structures.

The specimens have been observed using a JEOL F-200 operating a 200 kV, collecting the images through the Gatan Rio16 CMOS camera.

3. Results and discussion

3.1. SLES aggregation as function of ionic strength and temperature

Measurements of surface tension γ as function of concentration were performed on **E2S** and E3S in water having both high degree of purity and industrial grade (Fig. S3). The SLES with high purity exhibit the typical trend expected for pure surfactants, namely a decrease of the γ values up to the critical micellar concentration (cmc) and a plateau at higher values than cmc. The values of the cmc inferred from the measurements are 3 mM and 1.3 mM for **E2S** and **E3S**, respectively. Decreasing of the SLES' cmc compared to SDS (cmc 8.2 mM) and as a function of the increasing number ethoxyl group have been also previously reported [42]. On the other hand, industrial grade SLES show a remarkable minimum before the plateau region. This feature indicates the presence of hydrophobic impurities. Although the presence of such minima does not allow a precise estimation of the cmc, we notice that the minima (that should be close to the cmc) are at much lower values with respect to the cmc of the pure compounds. This indicates that the heterogeneous composition of the industrial grade SLES – both in terms of impurities and polydispersity of SLES – anticipates the assembly process.

The self-assembly of **E1S**, **E2S** and **E3S** was studied as a function of increasing ionic strength provided by addition of NaCl. It is known that addition of salt favors the aggregation into supramolecular structures or structure transitions [9,43–48]. This is due to the ability of the ions to screen the charge heads, reducing the repulsions and helping the assembly. We analyzed samples of SLES 1 wt% and NaCl ranging from 0.5 to 6.0 wt%. DLS data show for all the surfactants an initial range of NaCl concentration where the hydrodynamic diameters (D_H) of the aggregates are overall constant (Fig. 1) and in the same size range previously reported [49,50] for SDS in water (diameter 3.5–4 nm). Such ranges span up to NaCl concentration of about 2 wt%, 2.5 wt% and 3.5 wt% for **E1S**, **E2S** and **E3S**, respectively. Once exceeded such NaCl thresholds, a roughly linear increase of D_H as a function of NaCl concentration is observed. A similar value of NaCl concentration (0.45 M) was previously reported as threshold for the micelle growth of SDS [51]. The ethoxylation degree of the surfactants remarkably affects the slope of the linear trend, which is larger the lower the number of ethoxyl groups. As a consequence of such different growth, the aggregates measured at the highest NaCl concentration (6 wt%) have consistently different size (D_H of about 89, 51 nm and 22 nm size for **E1S**, **E2S** and **E3S**, respectively).

For a comparison, the intensity autocorrelation functions and the related size distributions for pure and industrial SLES were analyzed. In particular we focused on samples of **E3S** at 1 wt% with NaCl 6 wt%. Concerning not filtered samples, we observed that the correlogram of the industrial grade SLES exhibited an additional slower decaying component, along with a main steep decay (Fig. S4). In parallel, some large particles of several microns were observed to coexist with the micelles for this sample, from the intensity weighted size distributions. These particles were absent in the pure surfactant solutions and were identified as impurities. The impurities were removed after filtration with membranes with pore size of 450 nm.

In the case of both not filtered and filtered samples, larger micellar sizes were measured for the pure surfactant solutions. Based on this outcome, we anticipate that the impurities were able to adsorb part of the surfactant in the industrial grade samples, thereby removing micelle building blocks and reducing micellar sizes.

Small angle X-ray scattering data were collected for all the three surfactants at the extremes and an intermediate value of the analyzed NaCl concentration range, namely 0.5 wt%, 2.5 wt% and 6.0 wt% (Fig. 2). The corresponding pair distance distribution functions P(r) were inferred. All the P(r) functions show oscillatory profiles, indicating a complex distribution of the electron density within the aggregates. Moreover, the P(r) functions well-fit the core-shell model for ionic micelles. In such a model the hydrophobic tails are placed in the inner part of the aggregate whereas the ether groups and charged heads arrange at the external shell towards the aqueous medium. This structure results in a highly varying electron density across the cross-section: i) the electron density of the inner core is lower than that of the aqueous solvent, due to the hydrophobic chains only containing carbon and hydrogen and being packed with lower density; ii) the external corona electron density is higher than that of the aqueous solvent due to the presence of both hydrophilic moieties of the heads and condensed counterions.

The analysis of the P(r) functions shows a significant trend at values higher than 6 nm (inferred by SAXS data in the 0.1–3 nm^{-1} q range). For samples at NaCl 0.5 wt% (0.09 M), the values are slightly negative before approaching zero at the maximum size; this behavior is more pronounced moving in the series **E1S** <**E2S**< **E3S**. The same feature is instead no longer observable in the samples at NaCl 2.5 wt% (0.43 M) and 6.0 wt% (1.0 M). Negative P(r) values at high distances are usually ascribable to repulsive contributions in the structure factor [45].

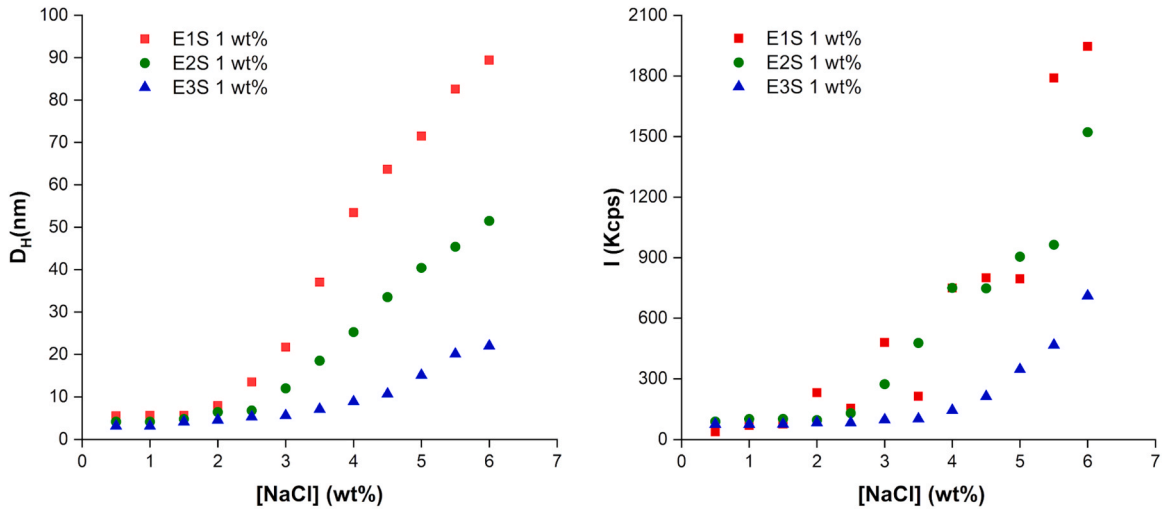

Fig. 1. Hydrodynamic diameter (left) and light scattered intensity (right) of E1S (squares), E2S (circles) and E3S (triangles) at 1 wt% in water as a function of NaCl concentration. The standard deviation is between 0.1 and 0.4 nm.

Therefore, NaCl fully screens the charged surface of the SLES structures only at the highest considered concentration values [52,53]. The observed screening threshold of NaCl concentration is in agreement with previous simulation studies on micelles of ionic surfactants that indicated Coulomb potential repulsion up to 0.1 M of NaCl [54].

For the samples at NaCl concentration of 6.0 wt%, the P(r) becomes strongly asymmetric, developing a tail at long distances. The elongation of such tail is evident for **E1S** and decreases by increasing the ethoxylation degree. The increasing asymmetry of the P(r) shape suggests the unidirectional growth of the aggregates from spherical to elongated wormlike micelles. Consistently, the initial power law observed in the 0.15–0.3 nm^{-1} q range of the SAXS data (Table S1) shows a trend towards a more negative exponent with increasing NaCl concentration and it is close to − 1 for **E1S** at NaCl 6%, as expected for rod-like geometry. This interpretation agrees with the increase of the DLS hydrodynamic diameters and scattered light intensities observed in Fig. 1. The pair distance distribution of the cross-section $P_{CS}(r)$ was also obtained (Fig. S5) by applying the indirect Fourier transform to I(q)·q in the assumption of rod-like object, indicating an overall cross-section size within 6 nm. Such value was assumed as a rod diameter to estimate an approximate length of the elongated micelles from the experimental hydrodynamic radii R_h values measured by DLS (Fig. 3) [55,56].

In light of this preliminary model-independent analysis, and in order to highlight structural differences among the micelles of the analyzed surfactants, the intensity vs. q curves were fitted according to analytical models. For the samples at NaCl concentration of 0.5 wt% the form factor of a core-shell sphere including a Hayter-Penfold structure factor for a screened Coulomb potential was assumed. For the samples at NaCl concentration of 6.0 wt%. the form factor of a core-shell ellipsoid or cylinder was adopted. A detailed comment about the modeling approach and the variability of the best-fitting parameters (e.g. different assumptions on the composition and molecular volumes for the core and the shell of the micelles), is reported as Supporting Information. Representative fits to the experimental data are reported in Fig. 4 and a consistent comparison of the structural parameters among the surfactants is reported in Tables S3-S5.

For the behavior at low NaCl content, the modeling results agree with a slight increase of the radius of the spherical micelles when increasing the average number of ethoxy units in the hydrophilic head. If the core radius is kept constant, such increase is reflected in an increase of only the shell thickness, which should accommodate a larger hydrophilic portion. Concurrently, a slight decrease of the best-fit scattering length density is obtained, but less than expected from the estimated electron densities of the dry polar heads (Table S2), and therefore also implies a slight decrease of water fraction.

For the micellar structure at high NaCl concentration (6%), the optimized values of the dimensional parameters highlight that a transition towards elongated micelles clearly occurs for **E1S**, while the SAXS data of **E2S** and **E3S** in NaCl 6% are best described by short ellipsoidal or cylindrical micelles, with progressively smaller axis ratio or length. The overall cross-section sizes do not undergo marked changes, but it could be appreciated (especially if the same scattering length density of the hydrophilic shell is assumed) that the rod-like geometry implies a shorter radius of the core compared to the globular geometry. The fact that the transition from globular to rodlike micelles induced by the addition of salt involves a decrease of the shorter micellar radius has indeed been observed also for SDS by SANS [56] and SAXS [57] and in that case it decreased from 1.7 ± 0.1 nm in absence of added salt to 1.4 ± 0.1 nm after the transition to rod-like geometry. We observed similar values for the core radius in case of **E1S**, while for **E2S** and **E3S** the cross-section sizes remain progressively closer to those observed in absence of salt.

The SAXS data for the two **E3S** samples at NaCl 6% (industrial grade and from synthesis) are indeed very different (Fig. S5, B) and the pure sample from synthesis at high NaCl concentration contains much larger aggregates, which could be better described according to a worm-like cylinder model (Table S6), being the initial slope more negative than the one expected for rigid rods. We also collected SAXS data on commercially available pure **E2S** and **E3S** and also in these cases the profiles drastically change for NaCl 6%, indicating a more pronounced micellar growth at high salt concentration compared to what is observed on an industrial grade mixture **(**Fig. S7**)**.

The transition from spherical to elongated aggregates and its readiness to occur more in **E1S** and **E2S** than **E3S**, can be also interpreted in terms of molecular packing parameter *P*. *P* is a parameter that relates the molecular structure of the surfactants with the morphology of the aggregates. It is defined as $v/a_e l$, where v and l are the volume and the length of the surfactant tail, respectively, whereas a_e is the equilibrium area per molecule occupied by the headgroup. Small *P* values (<1/3) gives rise to spherical micelles. On the other hands, increasing *P* values leads to the formation of wormlike micelles (P = 1/3–1/2), vesicles (P = 1/2–1) and inverted micelles (P > 1).

In agreement with the experimental data, the *P* equation predicts that the spherical to worm-like structural transition is easier the lower the number of the ethoxy groups since both l and a_e should decrease. However, at low NaCl concentration, from the experimental data it turns out that a_e value is still too high for having aggregates elongation even for **E1S**. Therefore, the charge screening of increasing ionic strength is

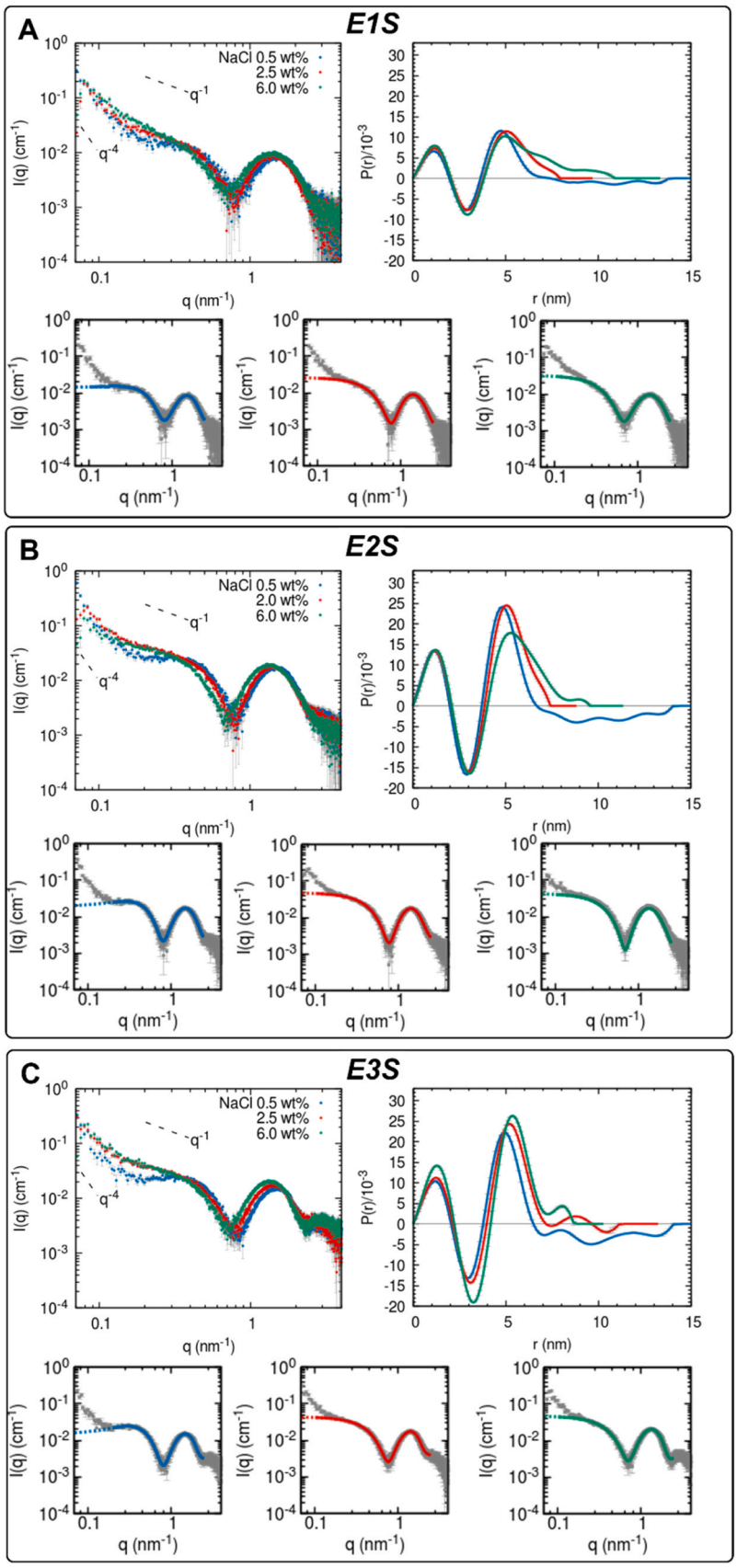

Fig. 2. SAXS intensity curves, P(r) and corresponding fits of E1S (A), E2S (B), E3S (C) at 1 wt% and different NaCl solution concentrations.

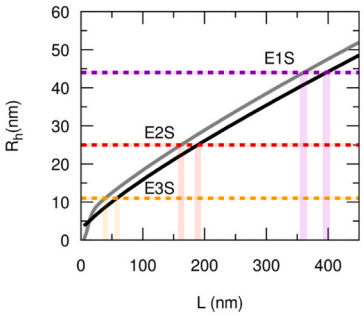

Sample	R_h (nm)	L (nm)[1]	L (nm)[2]
E1S 1% NaCl 6%	44.5 ± 0.5	360 ± 6	397 ± 6
E2S 1% NaCl 6%	25.5 ± 0.5	162 ± 5	190 ± 5
E3S 1% NaCl 6%	11 ± 0.5	39 ± 4	58 ± 4

(industrial grade mixtures)

[1]Equation $R_h(L) = \frac{L}{2\ln\left(\frac{2L}{d}\right) - 0.19 - \frac{8.24}{\ln\left(\frac{2L}{d}\right)} + \frac{12}{\left(\ln\left(\frac{2L}{d}\right)\right)^2}}$ (Broesma), d= 6 nm.

[2]Equation $R_h(L) = \frac{L}{2\ln\left(\frac{2L}{d}\right) + 0.312 + \frac{0.565d}{L} - \frac{0.1d^2}{L^2}}$ (Tirado), d = 6 nm.

Fig. 3. Theoretical trend of the hydrodynamic radii vs rod length according to the equations suggested by Broesma and Tirado (left, gray and black lines respectively). Extrapolation of the length of the SLES aggregates in NaCl 6% (left, continuous vertical lines) by using the experimental values of hydrodynamic radii measured by DLS (left, horizontal dashed lines). The results of the extrapolation process are summarized in the table (right).

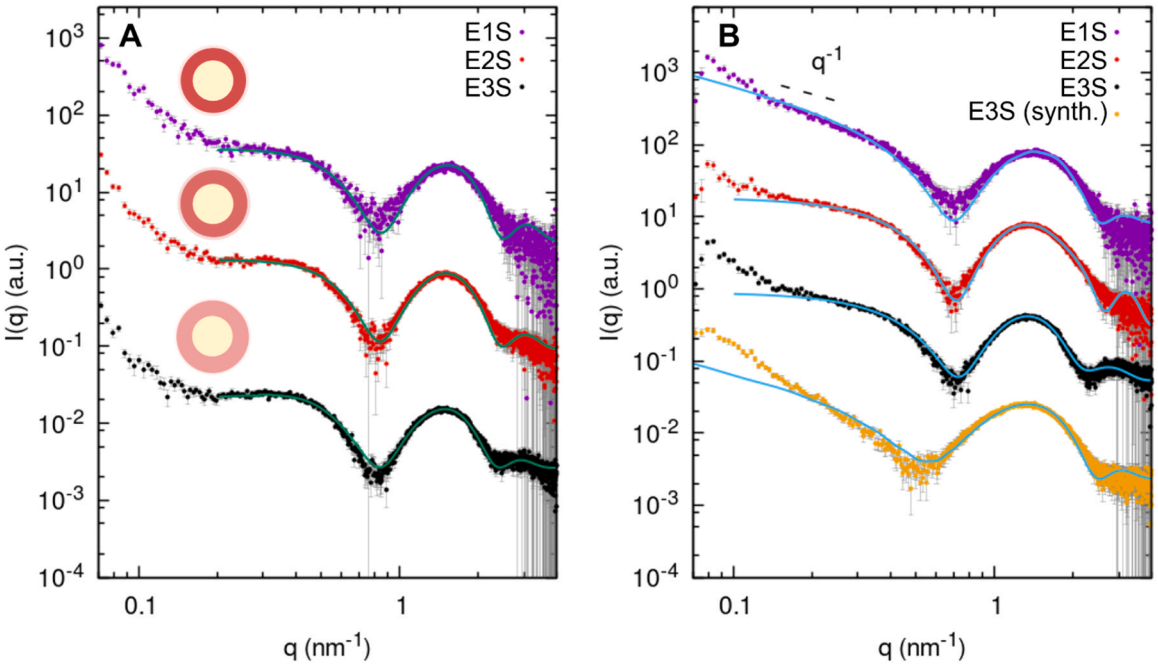

Fig. 4. Fits of the experimental SAXS curves (dots) for the E1S, E2S, and E3S samples at NaCl 0.5 wt% (A) and 6 wt% (B). Curves fits in A (green lines) were performed by using the form factor of a core-shell sphere, a screened Coulomb potential structure factor and a core radius value of 1.79 nm. Curves fits in B (cyan lines) were performed by using the form factor of a core-shell cylinder and by keeping the scattering length density of the shell constant to $10.86 \cdot 10^{-4}$ nm^{-2}. All the details on the model parameters are reported in Tables S3A and S5B.

needed to further decrease a_e and induce the transition to elongated micelles thereof. The effect of the ionic strength in decreasing a_e value and giving rise to elongated micelles is highly efficient in **E1S** and **E2S**, as also previously displayed by Zoeller and Blankschtein for the purified surfactants [29]. They also showed that such effect vanishes in **E4S**, **E5S** and **E6S** [29]. For the first time, reporting a systematic investigation of **E3S**, we prove that **E3S** is the borderline species in the series. For this surfactant, a globular to rod-like aggregate transition can still be appreciated from DLS data on the industrial grade mixture of **E3S** upon furnishing consistent ionic strength values and is also strongly suggested by the SAXS analysis of purified **E3S**.

TEM measurements were collected on pure **E3S** both in water and in NaCl 6 wt%, trying to image the morphological changes as a function of the added salt. Within the limits of possible structural modifications induced by the TEM grid preparation (e.g. drying and vacuum, see Materials and Methods section), the microscopy images are in acceptable agreement with the scattering data. The structures imaged in the sample in water are quite homogenous in size and shape, having regular circular profiles and an average diameter size of 4.6 ± 0.9 nm (Fig. S8 **A**). The structures observed in the sample with high salt concentration are instead bigger and more polydisperse (average diameter 14.7 ± 6.8 nm), presenting a much more irregular globular morphology. (Fig. S8 **B**).

Aggregates of SLES 1% in NaCl 6 wt% were subjected to temperature increases (Fig. 5). DLS data showed a decrease of the **E1S** and **E2S** aggregates' size in the 32–60 °C range. The D_H values at 60 °C for **E1S** and **E2S** aggregates are 40.2 nm and 36.3 nm, respectively. These dimensions, although smaller than the initial ones, still indicate an aggregation degree higher than the primary micelles. The micelle sizes of SDS reported in the literature seem to show a more pronounced decreasing trend as a function of the temperature. At the highest reported NaCl concentration (0.6 M) the micelle sizes approach the value ascribed to the primary spherical micelles (about 6 nm) at 60 °C [58].

On the other hand, **E3S** aggregates are highly stable and do not show sensitive size variation with the temperature increase.

3.2. *E3S assembly in presence of the typical formulation stabilizer TMBA*

Assembly of **E3S** samples with NaCl 1 wt%, 2.5 wt% and 6 wt% were studied as a function of addition of the **TMBA** (Fig. 6 **A, B**).

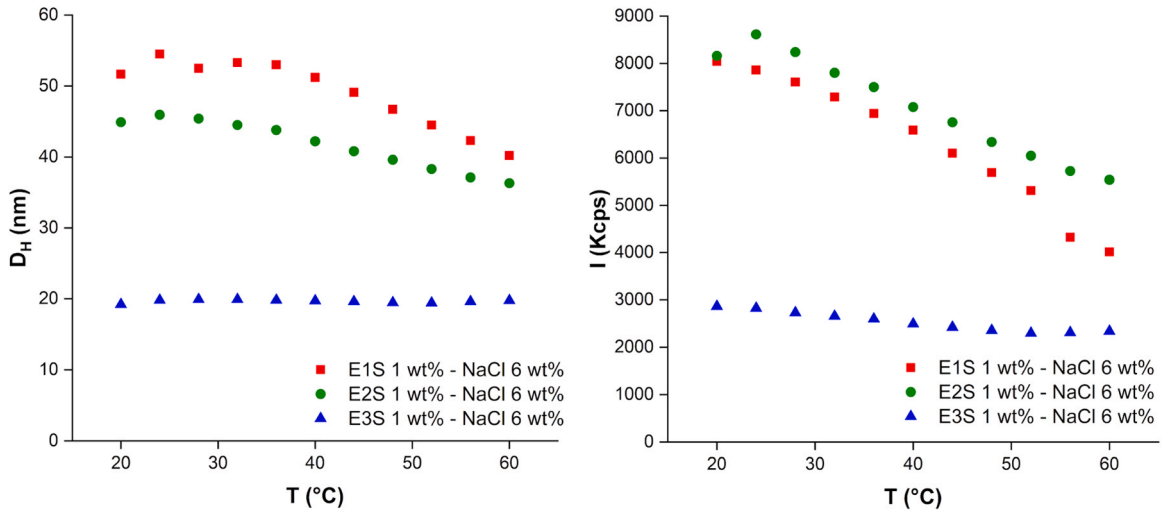

Fig. 5. Hydrodynamic diameter (left) and light scattered intensity (right) of E1S (circles), E2S (triangles) and E3S (squares) at 1 wt% in NaCl solution 6 wt% as a function of the temperature. The standard deviation is between 0.1 e 0.4.

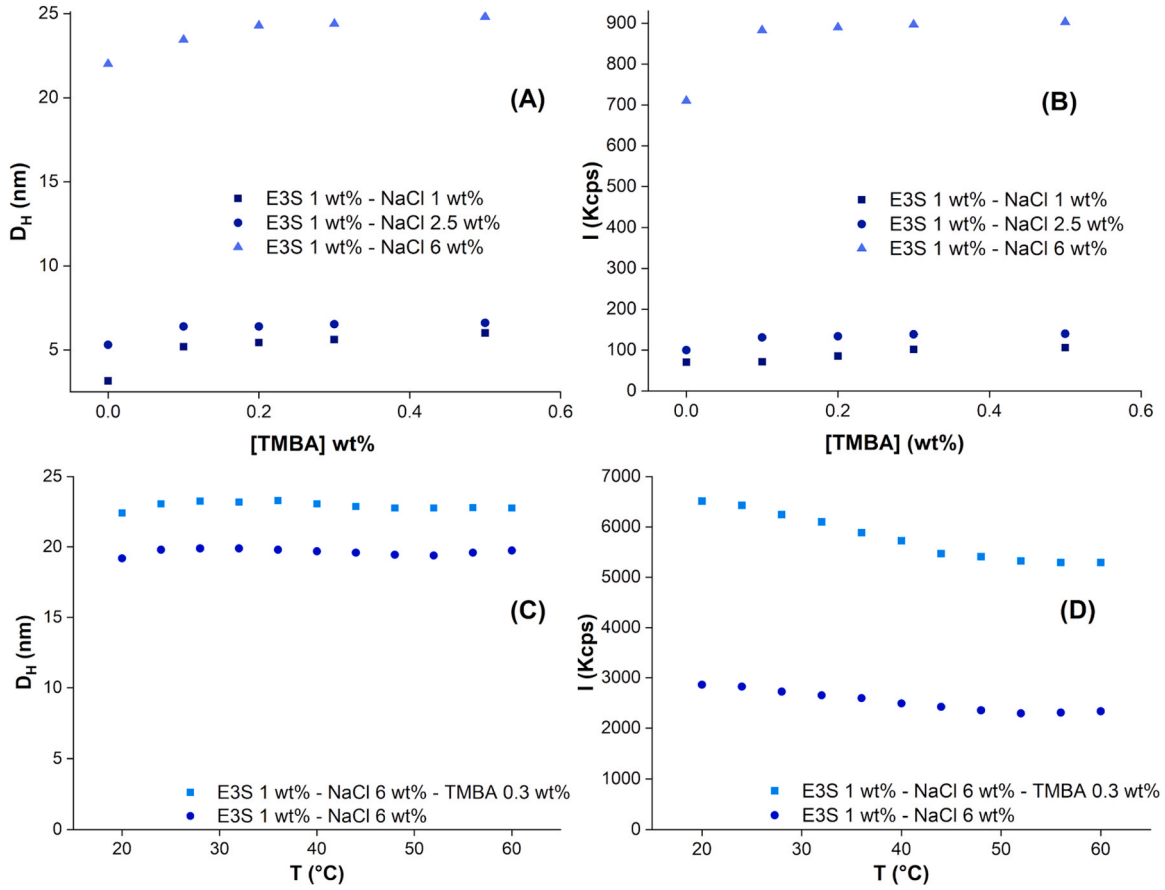

Fig. 6. Hydrodynamic diameters (A) and light scattered intensity (B) of E3S at 1 wt% in NaCl solution 1 wt% (squares), 2.5 wt% (circles) and 6 wt% (triangles) as a function of TMBA concentration. Hydrodynamic diameters (C) and light scattered intensity (D) of E3S at 1 wt% in NaCl solution 6 wt% with (squares) and without (circles) added TMBA 0.3 wt% as a function of the temperature. The standard deviation is between 0.1 and 0.3.

DLS data do not show significant variation of the overall aggregate size. Similarly, SAXS derived $P_{CS}(r)$ curves are basically invariant compared to the analogues systems without **TMBA** (Fig. 7), suggesting that the hydrotrope has no substantial effect in the core-shell structure of the micelles (SAXS models in Table S6). A change of the initial slope of the SAXS profiles with **TMBA** contents 0.2% and 0.3% towards a power law with less negative exponent (close to q^{-1}) could suggest an increased rigidity without substantial variations of the overall hydrodynamic size, apart from a slight increase as detected by DLS. The temperature increase (Fig. 6 **C**) has no relevant effect on the D_H values. All these data indicate a not relevant interaction among the two components.

In order to assess the hypothetical interaction between **E3S** and

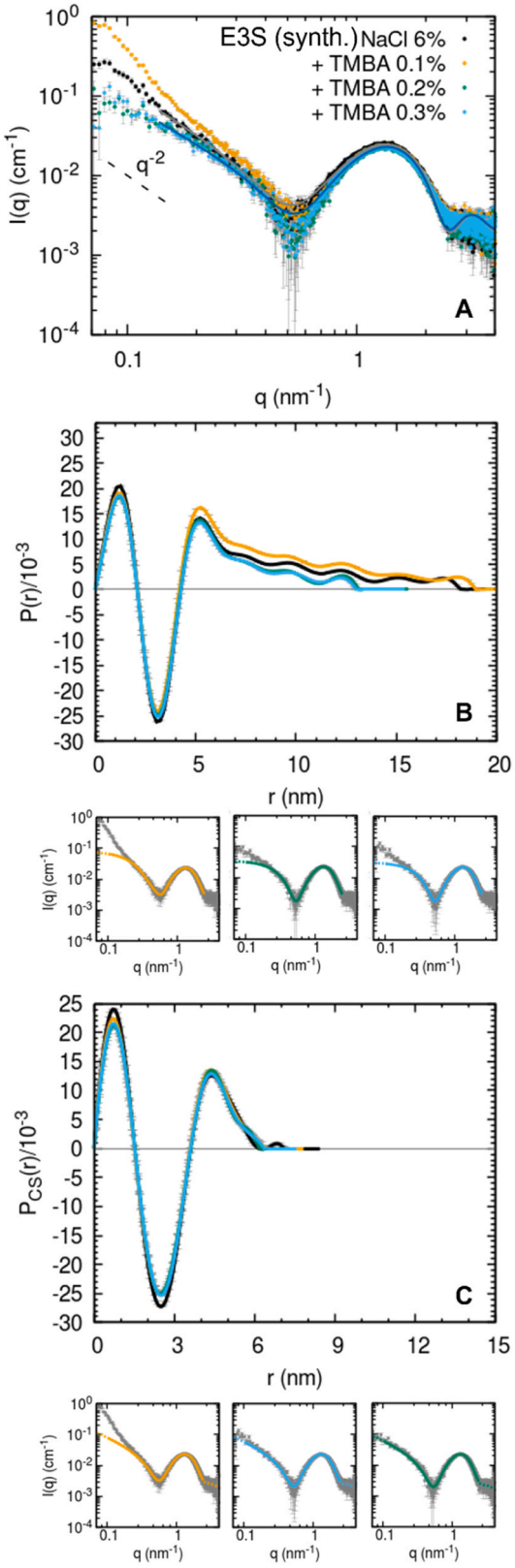

Fig. 7. SAXS analysis of E3S at 1 wt% in NaCl solution 6 wt% with increasing content of TMBA (0% black, 0.1% orange, 0.2% green, 0.3% light blue) Experimental SAXS profiles (A, dots) and calculated model profiles according to core-shell worm-like micelles (A, lines). Best-fitting parameters are reported in Table S6. P(r) and P(cs) transforms (B and C), along with the corresponding fits to the experimental profiles (insets).

TMBA, ^{1}H NMR and DOSY spectra were also collected. In Fig. 8 the resonances of the aliphatic protons of **E3S** are evidenced in blue (between 0.8 and 1.6 ppm) while the protons of **TMBA** are evidenced in red (the methoxy groups at 3.9 and 4.0 ppm while the aromatic protons at 7.45 ppm). In this experiment it is already observable that the two molecules possess different rotational mobility as assessed by the half-height width (HHW) of their resonances. HHWs are inversely proportional to relaxation time T_2, which is strongly influenced by the correlation time τ_C. This parameter is indicative of the rotational mobility of a single molecular group, and it can be employed to evaluate the relative mobility of molecules. Specifically, broader resonances are originated by slower and more hindered protons [59]. The resonance whose HHW is the broadest is relative to the $(CH_2)_n$ of **E3S** (11.92 Hz) while the aromatic CH of **TMBA** are narrower (5.32 Hz), and this difference is sufficient to hypothesize that the two molecules are not associated in this solvent. The DOSY spectrum confirmed this hypothesis since, as observed in figure 4.24b, the molecules showed that the coefficient of translational diffusion much higher for TMBA (logD = −9.15) than **E3S** (logD = −10.1). All these data further assess a lack of interaction and independent diffusion processes in solution of **TMBA** and **E3S** aggregates.

4. Conclusions

The work details the effect of ionic strength, temperature and addition of stabilizing species on the self-assembly properties of SLES having ether groups ranging from 1 to 3.

It was already reported that the size of **E1S** and **E2S** aggregates grows upon NaCl addition [29]. We further prove this aspect by enlarging the analyzed range of NaCl concentration and giving a detailed morphological description of the aggregate (i.e. transition from core-shell spheres to core-shell elongated structures) by SAXS data analysis.

Moreover, we provided for the first time a systematic study of **E3S** aggregation that is one of the most used SLES species in the formulation. Our data showed that **E3S** is a borderline species, i.e. the SLES with the highest number of ethoxyl groups still capable to give elongation of the aggregates at high ionic strength value. This behavior is observed both in the industrial grade and highly pure **E3S**. The industrial grade **SLES** exhibit a significant minimum of the surface tension as a function of surfactant concentration, before the plateau region, at lower values with respect to the cmc of the pure compounds, indicating the presence of hydrophobic impurities, which anticipate the self-assembly of the system. Impurities are also detected in unfiltered samples of the industrial grade **SLES** as large aggregates, which are supposed to partially adsorb the surfactant molecules.

A further innovative aspect of this work concerns the evidence of the high stability of the aggregates, especially **E3S**, as a function of increasing temperature. To the best of our knowledge, temperature studies of pure SLES aggregates are completely missing in the literature. Such data could be valuable for a basic understanding of SLES behavior in several real applications since temperature is an important parameter in industrial processes involving SLES based products (e.g. washing of surfaces and fabrics) [60–62]. Lastly, we proved that the **E3S** aggregates and **TMBA**, a known molecule used as stabilizer in some detergent, do not show significant and direct interactions. This suggests that some long-term transformations, induced by the dispersed **TMBA**, are responsible for the poor stability with time of some commercial formulations, revealed by industries.

Declaration of Competing Interest

The authors declare the following financial interests/personal relationships which may be considered as potential competing interests: Maria Chiara di Gregorio reports financial support was provided by Government of Italy Ministry of Education University and Research.

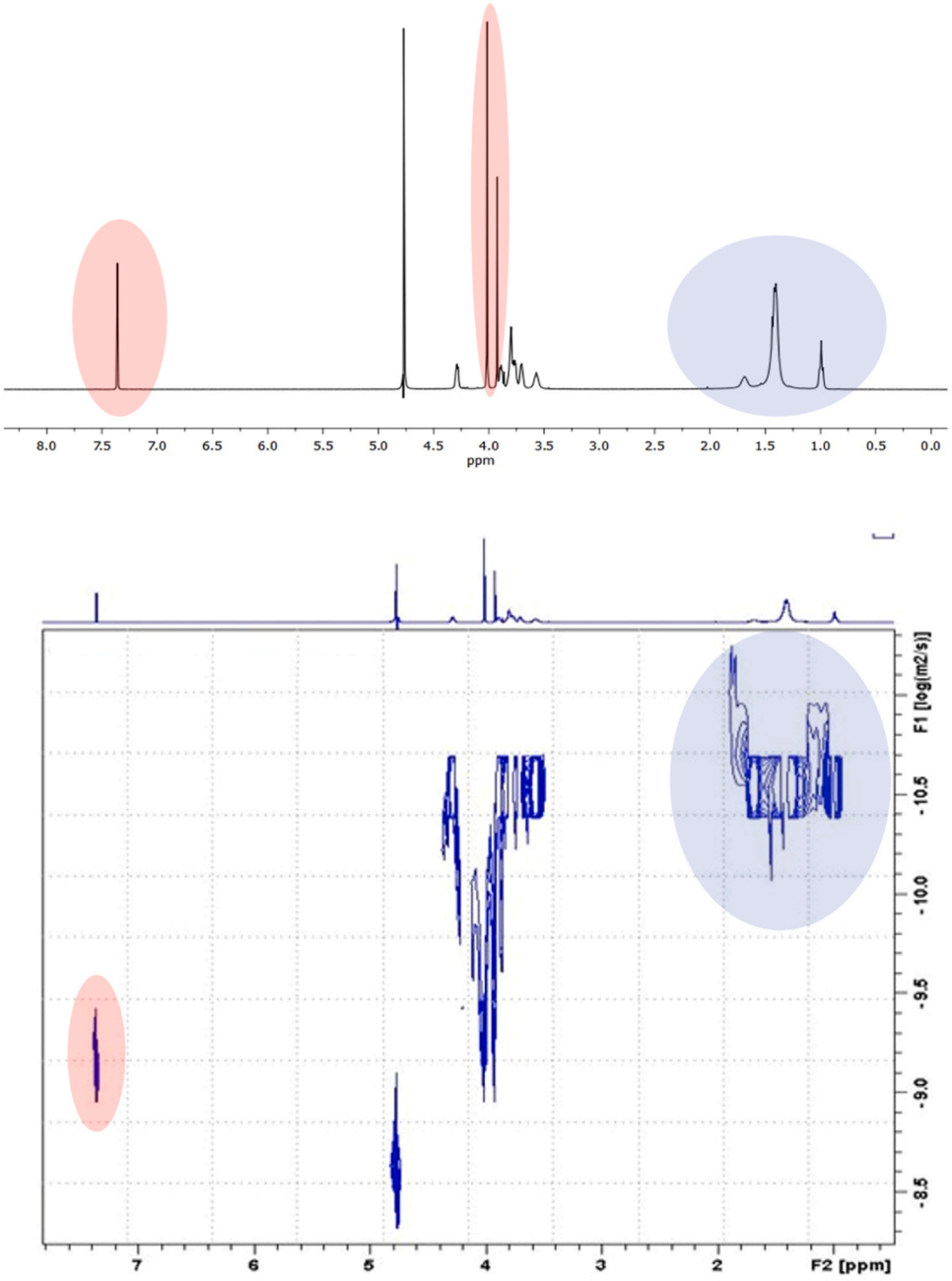

Fig. 8. H–NMR (top) and DOSY (bottom) spectra of the sample comprising of E3S 1 wt%, NaCl 6 wt% and TMBA 0.2 wt%.

Data availability

No data was used for the research described in the article.

Acknowledgements

This work is in memory of our dearest collegue Prof. N. V. Pavel. Our everlasting gratitude for his scientific and human contribution to our group. The MAX IV laboratory, Lund, Sweden is acknowledged for providing SAXS beamtime at the I911–4 beamline and the local contact S. Lages for support. We thank K. Schillén and M. Gubitosi for valuable help during the SAXS measurements. M. C. di Gregorio acknowledges support from the programme "Rita Levi Montalcini for young researchers" of the Italian Ministry of University and Research. A.D.G. acknowledges co-financing of Sapienza University of Rome and the European Union—FSE-REACT-EU, PON Research and Innovation 2014–2020 DM1062/2021 for the RTD-A contract.

Appendix A. Supporting information

Supplementary data associated with this article can be found in the online version at doi:10.1016/j.colsurfa.2024.133375.

References

[1] Industrial Cleaning Chemicals Market by Ingredient Type (Surfactants, Solvents, Chelating Agents, Ph Regulators, Solublizers/ Hydrotropes, Enzymes), Product Type, and Region (APAC,North America, Europe, MEA, South America) - Global Forecast to 2026 ⟨https://www.marketsandmarkets.com/Market-Reports/industrial-institutional-cleaning-chemicals-market-52902227.html⟩.

[2] C.B.B. Farias, F.C.G. Almeida, I.A. Silva, T.C. Souza, H.M. Meira, R. de C.F. Soares da Silva, J.M. Luna, V.A. Santos, A. Converti, I.M. Banat, et al., Production of green surfactants: market prospects, Electron. J. Biotechnol. 51 (2021) 28–39.

[3] G. Mallamaci, B. Brugnoli, A. Mariano, A. Scotto, A. Piozzi, V. Di, E. Sturabotti, S. Alfano, I. Francolini, Surface modification of polyester films with polyfunctional amines: effect on bacterial biofilm formation, Surf. Interfaces 39 (2024) 102924.
[4] G.O. Bianchetti, C.L. Devlin, K.R. Seddon, Bleaching systems in domestic laundry detergents: a review, RSC Adv. 5 (2015) 65365–65384.
[5] N.M. Khashab, F. Caruso, The future of healthcare materials, Chem. Mater. 35 (2023) 364–365.
[6] F. Polli, C. D'Agostino, R. Zumpano, V. De Martino, G. Favero, L. Colangelo, S. Minisola, F. Mazzei, ASu@MNPs-based electrochemical immunosensor for vitamin D3 serum samples analysis, Talanta 251 (2023) 123755.
[7] M. Consiglio, Di, E. Sturabotti, B. Brugnoli, A. Piozzi, L.M. Migneco, I. Francolini, Synthesis of sustainable Eugenol/Hydroxyethylmethacrylate-based polymers with antioxidant and antimicrobial properties, Polym. Chem. 14 (2023) 432–442.
[8] R. Zumpano, M. Manghisi, F. Polli, C. D'Agostino, F. Ietto, G. Favero, F. Mazzei, Label-free magnetic nanoparticles-based electrochemical immunosensor for Atrazine detection, Anal. Bioanal. Chem. 414 (2022) 2055–2064.
[9] G. Du, D. Belić, A. Del Giudice, V. Alfredsson, A.M. Carnerup, K. Zhu, B. Nyström, Y. Wang, L. Galantini, K. Schillén, Condensed supramolecular helices: the twisted sisters of DNA, Angew. Chemie Int. Ed. 61 (2022) 1–8.
[10] S.P. Chaudhari, R.P. Dugar, Application of surfactants in solid dispersion technology for improving solubility of poorly water soluble drugs, J. Drug Deliv. Sci. Technol. 41 (2017) 68–77.
[11] M.C. di Gregorio, E. Severoni, L. Travaglini, M. Gubitosi, S. Sennato, F. Mura, C. Redondo-Gómez, A. Jover, N.V. Pavel, L. Galantini, Bile acid derivative-based catanionic mixtures: versatile tools for superficial charge modulation of supramolecular lamellae and nanotubes, Phys. Chem. Chem. Phys. 20 (2018) 18957–18968.
[12] J. Gao, J.M. Karp, R. Langer, N. Joshi, The future of drug delivery, Chem. Mater. 35 (2023) 359–363.
[13] S. Chowdhury, S. Shrivastava, A. Kakati, J.S. Sangwai, Comprehensive review on the role of surfactants in the chemical enhanced oil recovery process, Ind. Eng. Chem. Res. 61 (2022) 21–64.
[14] O. Massarweh, A.S. Abushaikha, The use of surfactants in enhanced oil recovery: a review of recent advances, Energy Rep. 6 (2020) 3150–3178.
[15] Sodium Lauryl Sulfate Market Size, Share and Industry Analysis Report by Product (Liquid, Dry [Powder, Needles, Granules]) and Application (Dish Washing Liquids, Household Detergents & Cleaners, Industrial Cleaners, Personal Care Products), Regional Outlo. ⟨https://www.gminsights.com/industry-analysis/sodium-lauryl-sulfate-SLS-market⟩.
[16] A. Barra Caracciolo, M. Cardoni, T. Pescatore, L. Patrolecco, Characteristics and environmental fate of the anionic surfactant sodium Lauryl ether sulphate (SLES) used as the main component in foaming agents for mechanized tunnelling, Environ. Pollut. 226 (2017) 94–103.
[17] K. Kosswig, Surfactants. Ullmann's Encyclopedia of Industrial Chemistry, John Wiley & Sons Ltd., 2000.
[18] D. Balzer, S. Varwig, M. Weihrauch, Viscoelasticity of personal care products, Colloids Surf. A Physicochem. Eng. Asp. 99 (1995) 233–246.
[19] R.L. Hendrikse, A.E. Bayly, P.K. Jimack, Studying the structure of Sodium Lauryl ether sulfate solutions using dissipative particle dynamics, J. Phys. Chem. B 126 (2022) 8058–8071.
[20] A. Barra Caracciolo, N. Ademollo, M. Cardoni, A. Di Giulio, P. Grenni, T. Pescatore, J. Rauseo, L. Patrolecco, Assessment of biodegradation of the anionic surfactant sodium Lauryl ether sulphate used in two foaming agents for mechanized tunnelling, Excav. J. Hazard. Mater. 365 (2019) 538–545.
[21] A. Patist, P.D.T. Huibers, B. Deneka, D.O. Shah, Effect of long chain alcohols on micellar relaxation time and foaming properties of Sodium Dodecyl sulfate solutions alexander, Langmuir 14 (1998) 4471–4474.
[22] C. Ade-Browne, M. Mirzamani, A. Dawn, S. Qian, R.G. Thompson, R.W. Glenn, H. Kumari, Effect of Ethoxylation and Lauryl Alcohol on the self-assembly of Sodium Laurylsulfate: significant structural and rheological transformation, Colloids Surf. A Physicochem. Eng. Asp. 595 (2020) 124704.
[23] G.S. Georgieva, S.E. Anachkov, I. Lieberwirth, K. Koynov, P.A. Kralchevsky, Synergistic growth of giant wormlike Micelles in ternary mixed surfactant solutions: effect of octanoic acid, Langmuir 32 (2016) 12885–12893.
[24] K. Golemanov, N.D. Denkov, N.D. Tcholakova, M. Vethamuthu, A. Lips, Surfactant mixtures for control of bubble surface mobility in foam studies, Langmuir 24 (2008) 9956–9961.
[25] J.R. Liley, J. Penfold, R.K. Thomas, I.M. Tucker, J.T. Petkov, P.S. Stevenson, I. M. Banat, R. Marchant, M. Rudden, A. Terry, et al., Self-assembly in dilute mixtures of non-ionic and anionic surfactants and Rhamnolipd biosurfactants, J. Colloid Interface Sci. 487 (2017) 493–503.
[26] Y. Tang, Z. Liu, L. Zhu, Y. Han, Y. Wang, Aggregation behavior of Sodium Lauryl Ether Sulfate with a positively bicharged organic salt and effects of the mixture on fluorescent properties of conjugated polyelectrolytes, Langmuir 31 (2015) 2104–2111.
[27] N. Pandya, G. Rajput, D.S. Janni, G. Subramanyam, D. Ray, V. Aswal, D. Varade, SLES/CMEA mixed surfactant system: effect of electrolyte on interfacial behavior and microstructures in aqueous media, J. Mol. Liq. 325 (2021) 115096.
[28] D. Varade, S.C. Sharma, K. Aramaki, Viscoelastic behavior of surfactants worm-like micellar solution in the presence of alkanolamide, J. Colloid Interface Sci. 313 (2007) 680–685.
[29] N. Zoeller, D. Blankschtein, Experimental determination of Micelle shape and size in aqueous solutions of Dodecyl Ethoxy Sulfates, Langmuir 14 (1998) 7155–7165.
[30] F. Tokiwa, K. Ohki, Micellar properties of a series of Sodium Dodecylpolyoxyethylene sulfates from hydrodynamic data, J. Phys. Chem. 71 (1967) 1343–1348.
[31] A. Parker, W. Fieber, Viscoelasticity of anionic wormlike Micelles: effects of ionic strength and small hydrophobic molecules, Soft Matter 9 (2013) 1203–1213.
[32] A. Briatore, A. Gagliardini, M.A. Moss, O. Todini, Bleaching Composition Comprising Trimethoxy Benzoic Acid or a Salt Thereof. US-7910536-B2.
[33] V. Guida, B. Perfili, L. Sarcinelli, Colored Bleaching Composition. EP 2112218 B1 20110817.
[34] R. Paul, K.G. Chattaraj, S. Paul, Role of hydrotropes in sparingly soluble drug solubilization: insight from a molecular dynamics simulation and experimental perspectives, Langmuir 37 (2021) 4745–4762.
[35] C.V. Subbarao, I.P.K. Chakravarthy, A.V.S.L. Sai Bharadwaj, K.M.M. Prasad, Functions of hydrotropes in solutions, Chem. Eng. Technol. 35 (2012) 225–237.
[36] A. Labrador, Y. Cerenius, C. Svensson, K. Theodor, T. Plivelic, The yellow mini-hutch for SAXS experiments at MAX IV laboratory, J. Phys. Conf. Ser. 425 (part 7) (2013).
[37] A.P. Hammersley, S.O. Svensson, M. Hanfland, A.N. Fitch, D. Hausermann, Two-dimensional detector software: from real detector to idealised image or Two-theta scan, High. Press. Res. 14 (1996) 235–248.
[38] D. Orthaber, A. Bergmann, O. Glatter, SAXS experiments on absolute scale with Kratky systems using water as a secondary standard, J. Appl. Crystallogr. 33 (2) (2000) 218–225.
[39] S. Hansen, BayesApp: a web site for indirect transformation of small-angle scattering data, J. Appl. Crystallogr. 45 (3) (2012) 566–567.
[40] SasView, version 5.0.5, 2021 ⟨http://www.sasview.org/⟩.
[41] J. Kohlbrecher, I. Breßler, A. Barty, Updates in SASfit for fitting analytical expressions and numerical models to small-angle scattering patterns, J. Appl. Crystallogr. 55 (2022) 1677–1688.
[42] A. Del Regno, P.B. Warren, D.J. Bray, R.L. Anderson, Critical Micelle concentrations in surfactant mixtures and blends by simulation, J. Phys. Chem. B 125 (2021) 5983–5990.
[43] B. Lukanov, A. Firoozabadi, Specific ion effects on the self-assembly of ionic surfactants: a molecular thermodynamic theory of micellization with dispersion forces, Langmuir 30 (2014) 6373–6383.
[44] J.V. Trillo, A. Jover, L. Galantini, J.V. Tato, V.H. Soto, F. Meijide, M.C. di Gregorio, S. de Frutos, Self-aggregation mechanism of a naphthylamide cationic derivative of cholic acid from fibers to tubules, RSC Adv. 4 (2013) 5598–5606.
[45] A. Jover, F. Fraga, F. Meijide, J.V. Tato, J. Cautela, A.Del Giudice, M.C. di Gregorio, Revealing the complex self-assembly behaviour of sodium deoxycholate in aqueous solution, J. Colloid Interface Sci. 604 (2021) 415–428.
[46] M.C. di Gregorio, M. Elsousou, Q. Wen, L.J.W. Shimon, V. Brumfeld, L. Houben, M. Lahav, M.E. van der Boom, Molecular cannibalism: sacrificial materials as precursors for hollow and multidomain single crystals, Nat. Commun. 12 (2021) 957.
[47] H. Nasi, M.C. di Gregorio, Q. Wen, L.J.W. Shimon, I. Kaplan-Ashiri, T. Bendikov, G. Leitus, M. Kazes, D. Oron, M. Lahav, et al., Directing the morphology, packing, and properties of chiral metal–organic frameworks by cation exchange, Angew. Chemie Int. Ed. 61 (2022) e202205238.
[48] M.C. di Gregorio, V. Singh, L.J.W. Shimon, M. Lahav, M.E. Van Der Boom, Crystallographic-morphological connections in star shaped metal-organic, frameworks. J. Am. Chem. Soc. 144 (2022) 22838–22843.
[49] M. Molero, R. Andreu, D. Gonzàlez, J.J. Calvente, G. López-Pérez, An isotropic model for micellar systems: application to sodium dodecyl sulfate solutions, Langmuir 17 (2) (2001) 314–322.
[50] C.D. Bruce, M.L. Berkowitz, L. Perera, M.D.E. Forbes, Molecular dynamics simulation of sodium dodecyl sulfate micelle in water: micellar structural characteristics and counterion distribution, J. Phys. Chem. B 106 (15) (2002) 3788–3793.
[51] S. Hayashi, S. Ikeda, Micelle size and shape of sodium dodecyl sulfate in concentrated sodium chloride solutions, J. Phys. Chem. 84 (1980) 744–751.
[52] G. Esposito, E. Giglio, N.V. Pavel, A. Zanobi, Size and shape of sodium deoxycholate micellar aggregates, J. Phys. Chem. 91 (1987) 356–362.
[53] L. Galantini, E. Giglio, A. Leonelli, N.V. Pavel, An integrated study of small-angle x-Ray scattering and dynamic light scattering on cylindrical micelles of sodium glycodeoxycholate, J. Phys. Chem. B 108 (2004) 3078–3085.
[54] L. Cannavacciuolo, J.S. Pedersen, P. Schurtenberger, Monte carlo simulation study of concentration effects and scattering functions for polyelectrolyte wormlike Micelles, Langmuir 18 (2002) 2922–2932.
[55] A. Ortega, J. Garcia De La Torre, Hydrodynamic properties of rodlike and dislike particles in dilute solution, J. Chem. Phys. 119 (2003) 9914–9919.
[56] S. Broersma, Viscous force and torque constants for a cylinder, J. Chem. Phys. 74 (1981) 6989–6990.
[57] G.V. Jensen, R. Lund, J. Gummel, T. Narayanan, J.S. Pedersen, Monitoring the transition from spherical to polymer-like surfactant micelles using small-angle x-ray scattering, Angew. Chem. Int. Ed. 53 (2014) 11524–11528.
[58] N.A. Mazer, G.B. Benedek, M.C. Carey, An investigation of the Micellar phase of sodium dodecyl sulfate in aqueous sodium chloride solutions using quasielastic light scattering spectroscopy, J. Phys. Chem. 80 (10) (1976) 1075–1085.
[59] X. Cui, S. Mao, M. Liu, H. Yuan, Y. Du, Mechanism of surfactant Micelle formation, Langmuir 24 (2008) 10771–10775.
[60] D.P. Bockmühl, J. Schages, L. Rehberg, Laundry and textile hygiene in healthcare and beyond, Microb. Cell 6 (2019) 299–306.
[61] S. Rotzler, M. von Krshiwoblozki, M. Schneider-Ramelow, Washability of e-textiles: current testing practices and the need for standardization, Text. Res. J. 91 (2021) 2401–2417.
[62] A. Bashir, A. Sharifi Haddad, R. Rafati, A review of fluid displacement mechanisms in surfactant-based chemical enhanced oil recovery processes: analyses of key influencing factors, Pet. Sci. 19 (2022) 1211–1235.